Research Article | Vol. 55, No. 33 / November 20 2016 / Applied Optics 9459

applied optics

Calibration of oblique-incidence reflectivity difference for label-free detection of a molecular layer

CHENGGANG ZHU,[1] RU CHEN,[1] YUZHANGYANG ZHU,[1] XU WANG,[2] XIANGDONG ZHU,[3] LAN MI,[1] FENGYUN ZHENG,[4] AND YIYAN FEI[1,*]

[1]Department of Optical Science and Engineering, Shanghai Engineering Research Center of Ultra-Precision Optical Manufacturing, Green Photoelectron Platform, Key Laboratory of Micro and Nano Photonic Structures (Ministry of Education), Fudan University, Shanghai 200433, China
[2]Department of Fundamental Courses, Wuxi Institute of Technology, Wuxi 214121, China
[3]Department of Physics, University of California, Davis, California 95616, USA
[4]Institutes of Biomedical Science, Fudan University, Shanghai 200032, China
*Corresponding author: fyy@fudan.edu.cn

Received 24 August 2016; revised 19 October 2016; accepted 20 October 2016; posted 20 October 2016 (Doc. ID 270382); published 16 November 2016

Oblique-incidence reflectivity difference (OI-RD) is a form of polarization-modulation ellipsometry that measures properties of thin films on a solid surface through the change in polarization state of light upon reflection from the surface. The measurement accuracy depends on the precision of the phase modulation amplitude and azimuthal alignments of key polarizing optical elements and, thus, requires careful calibration. In the present work, we describe robust methods of such calibrations that enable precise determination of the modulation amplitude and static retardation of a phase modulator and azimuths of key polarizing optics in an OI-RD system.

OCIS codes: (120.2130) Ellipsometry and polarimetry; (260.5430) Polarization; (120.5060) Phase modulation; (120.5050) Phase measurement.

http://dx.doi.org/10.1364/AO.55.009459

1. INTRODUCTION

Ellipsometry is a class of optical techniques widely used to measure the thickness and refractive index of thin films on solid surfaces through the measurement of polarization state change. In nulling ellipsometry [1], the intensity of a polarized light beam reflected from a solid surface is extinguished through azimuthal adjustments of polarization optics in the instrument. The azimuths of the polarization optics required to null the intensity at the detector are used to extract the change in the polarization state. To detect ellipsometry signals at frequencies away from $1/f$ noise, one typically uses polarization-modulation ellipsometry (PME) [2], in which a photo-elastic modulator (PEM) or electro-optic phase modulator (EOM) is utilized to introduce an oscillatory phase retardation along one major axis at the frequency Ω. As a result, the intensity of the detected ellipsometry signal consists of harmonics of Ω, and the first and second harmonic components are routinely used to extract the polarization change with an improved signal-to-noise ratio (SNR). OI-RD is a form of nulling PME [3,4]. Reflectivities for obliquely incident p- and s-polarized light change disproportionately in response to a change in thickness or dielectric response of the film. OI-RD directly measures such disproportional phase and amplitude changes using the first and second harmonics of the ellipsometry signal. OI-RD has been successfully applied by Zhu and coworkers to studies of a wide variety of materials and processes, including ion sputtering and thermal annealing [5,6], gas adsorption [3,7], epitaxial growth [8,9], electrochemical deposition [10,11], and optical biosensing [12–17].

OI-RD usually consists of a polarizer, a PEM, a phase shifter, and an analyzer. The polarizer generates a linear-polarized incident light beam, the PEM alters the light beam from p-polarized to s-polarized at the frequency Ω, and the phase shifter alters the static phase difference between the p- and s-polarized components. The analyzer mixes the two polarized components such that afterward the first and second harmonics of the detected signal yield information on the polarization state change. The PEM consists of a fused silica bar vibrating at a natural resonant frequency sustained by a piezoelectric transducer. The periodic stress produces an extra time-varying phase along the stressed axis. The precisions of the phase modulation amplitude and the azimuths of all of the polarizing optics affect the precision of the polarization state measurement. As a result, procedures need to be established to conveniently and precisely determine static and alternating phase retardation of the PEM and azimuths of key polarizing optics, and how precisions of these parameters quantitatively affect the extracted polarization changes.

In this work, we describe a set of calibration methods for OI-RD that (1) measure the modulation amplitude and static phase retardation of a PEM, and (2) set azimuths of the polarizer, PEM, phase shifter, and analyzer. Since a PEM is a stable device, part (1) needs to be performed only occasionally. Part (2) may be performed more frequently with the sample in place.

2. DESCRIPTION OF AN OI-RD SYSTEM

Figure 1 shows the schematic diagram of an OI-RD system [13,16,18–20]. With the polarizer azimuth P at 45°, the PEM azimuth M at 0°, the phase shifter azimuth PS at 0°, the analyzer azimuth A at 135°, and the PEM phase modulation $\varphi = \varphi_A \cos \Omega t$ ($\Omega = 2\pi f$, $f = 50$ kHz), the detected ellipsometry signal $I(t)$ is expressed as a function of the modulation frequency Ω,

$$I(t) = I(dc) + I(\Omega)\cos \Omega t + I(2\Omega)\cos 2\Omega t + \text{higher terms}. \tag{1}$$

The OI-RD system measures the first harmonic $I(\Omega)$ and the second harmonic $I(2\Omega)$ with lock-in amplifiers. If there are no errors in any of the azimuths, $I(\Omega)$ and $I(2\Omega)$ can be expressed as

$$I(\Omega) = -I_0\eta_1 J_1(\varphi_A)|r_p||r_s|\sin(\delta - \Phi_{ps} - \Phi_{sys}), \tag{2}$$

$$I(2\Omega) = I_0\eta_2 J_2(\varphi_A)|r_p||r_s|\cos(\delta - \Phi_{ps} - \Phi_{sys}). \tag{3}$$

I_0 is the intensity of the incident light beam. η_1 and η_2 are frequency-dependent amplification factors for the first harmonic and the second harmonic, respectively, of the entire detection electronics, including the transducer and cables. φ_A is the modulation amplitude of the PEM (in radians). $J_1(\varphi_A)$ and $J_2(\varphi_A)$ are Bessel functions of the first kind. $|r_p|$ and $|r_s|$ are

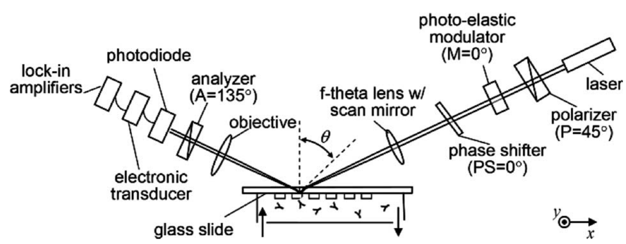

Fig. 1. Schematic diagram of OI-RD system particular for microarray detection. Polarization optics (polarizer, photo-elastic modulator (PEM), phase shifter, and analyzer) are used to analyze the polarization state change of light reflection from a microarray. Light scanning along the y direction achieved by a f-theta lens with a scan mirror and a translation stage, scanning along the x direction, provide the spatial resolution for the OI-RD system. Photodiode, electronic transducer, and lock-in amplifiers are used to measure light intensity. For accurate data reduction, the azimuths for the polarizer, PEM, phase shifter, and analyzer are set at $P = 45°$, $M = 0°$, $PS = 0°$, and $A = 135°$, respectively.

amplitudes of reflectivity for p- and s-polarized components, and $\delta = \Phi_p - \Phi_s$ is the phase difference between the p- and s-polarized components acquired upon reflection from the surface. Φ_{ps} is the adjustable phase difference between the p- and s-polarization introduced by the phase shifter, and Φ_{sys} is the phase difference between the p- and s-polarization contributed by all of the optical elements in the beam path other than the sample and the phase shifter.

Let δ_0 be the phase difference between the p- and s-polarization from the bare substrate surface. One can adjust Φ_{ps} until $\delta_0 - \Phi_{ps} - \Phi_{sys} = 0$, and the first harmonic $I(\Omega) = 0$ on the bare substrate surface. When a thin layer of molecules (thickness d) is subsequently added to the bare surface, the phase difference between the p- and s-polarization becomes δ, and the change $\Delta\delta = \delta - \delta_0$ can be determined using the resultant first harmonic and the second harmonic amplitudes;

$$I(\Omega) = -I_0\eta_1 J_1(\varphi_A)|r_p||r_s|\sin(\delta - \delta_0). \tag{4}$$

$$I(2\Omega) = I_0\eta_2 J_2(\varphi_A)|r_p||r_s|\cos(\delta - \delta_0). \tag{5}$$

When $\Delta\delta$ is small, the first harmonic is used to yield $\Delta\delta$. $\Delta\delta$ is related to the physical properties of the molecular layer, such as the thickness d as follows [13]:

$$\Delta\delta \cong \frac{-4\pi\sqrt{\epsilon_s}\cos\theta}{(\epsilon_0 - \epsilon_s)(\cot^2\theta - \epsilon_s/\epsilon_0)} \frac{(\epsilon_d - \epsilon_o)(\epsilon_d - \epsilon_s)}{\epsilon_d} \frac{d}{\lambda}. \tag{6}$$

λ is the wavelength of the light beam. ϵ_s, ϵ_0, and ϵ_d are the optical dielectric constants of the ambient, solid substrate, and molecular layer, respectively. θ is the incident angle on the substrate surface bearing samples. For detection on the interface of glass and water, we set $\theta = 37.5°$ for a betterSNR. Thus, in OI-RD, one measures the molecular thickness d through the detection of $\Delta\delta$.

Yet, Eqs. (2)–(5) are valid only when azimuths are set accurately at the specified values, i.e., $P = 45°$, $M = 0°$, $PS = 0°$, and $A = 135°$. In general, the first harmonic and the second harmonic depend on these azimuths as

$$\begin{aligned} I(\Omega) = {} & I_0\eta_1 J_1(\varphi_A)\sin 2(M - P) \\ & \times \left\{ |r_p||r_s|\sin 2A \begin{bmatrix} \cos 2PS\cos(\delta - \Phi_{sys})\sin\Phi_{ps} \\ -\sin(\delta - \Phi_{sys})\cos\Phi_{ps} \end{bmatrix} \right. \\ & \left. - \sin 2PS\sin\Phi_{ps}[|r_p|^2\cos^2 A - |r_s|^2\sin^2 A] \right\}, \end{aligned} \tag{7}$$

$$\begin{aligned} I(2\Omega) = {} & -I_0\eta_2 J_2(\varphi_A)\sin 2(M - P) \\ & \times \left\{ [|r_p|^2\cos^2 A - |r_s|^2\sin^2 A] \right. \\ & \times \begin{bmatrix} \cos 2PS\sin 2(M - PS) \\ +\sin 2PS\cos 2(M - PS)\cos\Phi_{ps} \end{bmatrix} + |r_p||r_s|\sin 2A \\ & \left. \times \begin{bmatrix} \sin 2PS\sin 2(M - PS)\cos(\delta - \Phi_{sys}) \\ -\cos 2PS\cos 2(M - PS)\cos(\delta - \Phi_{sys})\cos\Phi_{ps} \\ -\cos 2(M - PS)\sin(\delta - \Phi_{sys})\sin\Phi_{ps} \end{bmatrix} \right\}. \end{aligned} \tag{8}$$

Equations (7) and (8) show that $|r_p|^2 \cos^2 A - |r_s|^2 \sin^2 A$, $\sin(\delta - \Phi_{sys})$, and $\cos(\delta - \Phi_{sys})$ are generally coupled in both harmonics. If one still uses Eqs. (4) and (5) to calculate $\Delta\delta$, the result is no longer accurate unless the azimuths of all polarizing optics and the phase retardation from the PEM are carefully set or calibrated.

3. CALIBRATION OF THE PHOTO-ELASTIC MODULATOR

The PEM is a critical element in an OI-RD system. The modulation amplitude φ_A appears in the amplitudes of the first and the second harmonic signals. The calibration of φ_A can be performed in the straight–through configuration [21], as shown in Fig. 2, in which the sample is removed, and the PEM is placed between two crossed polarizers with transmission axes at 45° and 135° with respect to the modulation axis (i.e., the mechanically stressed axis). The detector is a photodiode with its output connected to an oscilloscope or to two lock-in amplifiers. For a phase modulation in the form of $\varphi = \varphi_A \cos \Omega t$, the light intensity at the detector is given by

$$I(t) = \frac{I_0}{2}[1 - \cos(\varphi_A \cos \Omega t)] = \frac{I_0}{2}[1 - \eta_0 J_0(\varphi_A) + 2\eta_2 J_2(\varphi_A) \cos 2\Omega t + \text{higher terms} \cdots]. \quad \textbf{(9)}$$

It consists of only even harmonics of modulation frequency. A number of features can be used to calibrate the modulation amplitude φ_A: (1) the distinctive waveform on the oscilloscope with φ_A being an integral multiple of π radians [22–24]; (2) the Bessel function zeros, such as $J_0(\varphi_A)$, being zero when φ_A is equal to 2.405, and $J_2(\varphi_A)$ being zero when φ_A is equal to 5.136; and (3) the Bessel function maxima with $J_1(\varphi_A)$ being maximized when φ_A is equal to 1.841 [25]. These are single-point calibration techniques. We propose a calibration method that involves curve fitting the entire waveform $\cos(\varphi_A \cos \Omega t)$ and is thus more accurate.

The function $\cos(\varphi_A \cos \Omega t)$ shows a "flat topped" and "flat bottomed" characteristic when φ_A is a multiple of π radians. By adjusting φ_A to give a "flat topped" or "flat bottomed" waveform by visual inspection, φ_A is equal to π within an accuracy of 1%–2% [22,26]. We find that the entire temporal waveform is sensitive to the modulation amplitude φ_A, and we can determine φ_A much more accurately by fitting the waveform to the function $\cos(\varphi_A \cos \Omega t)$ instead of by visual inspection. We set values of modulation amplitude φ_A^s on the PEM controller (PEM100, Hinds Instruments, USA) and record the corresponding waveforms with a digital oscilloscope. The waveforms are then fitted to function $\cos(\varphi_A \cos \Omega t)$ to yield the fitted modulation amplitude φ_A^f. Figure 3 shows the waveforms (open circles) obtained with set values φ_A^s and the corresponding fitting curves (solid lines) using the fitted φ_A^f. The fitted values φ_A^f are generally larger than the set values φ_A^s. Since the modulation amplitude φ_A is a linear function of the modulator voltage from the controller [27], it is reasonable that the relationship between the modulation amplitude setting value φ_A^s and the fitted value φ_A^f is linear. Figure 4 shows the linear

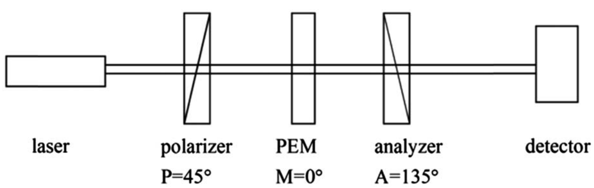

Fig. 2. Straight–through configuration to calibrate modulation amplitude φ_A and static phase retardation φ_0 of the PEM.

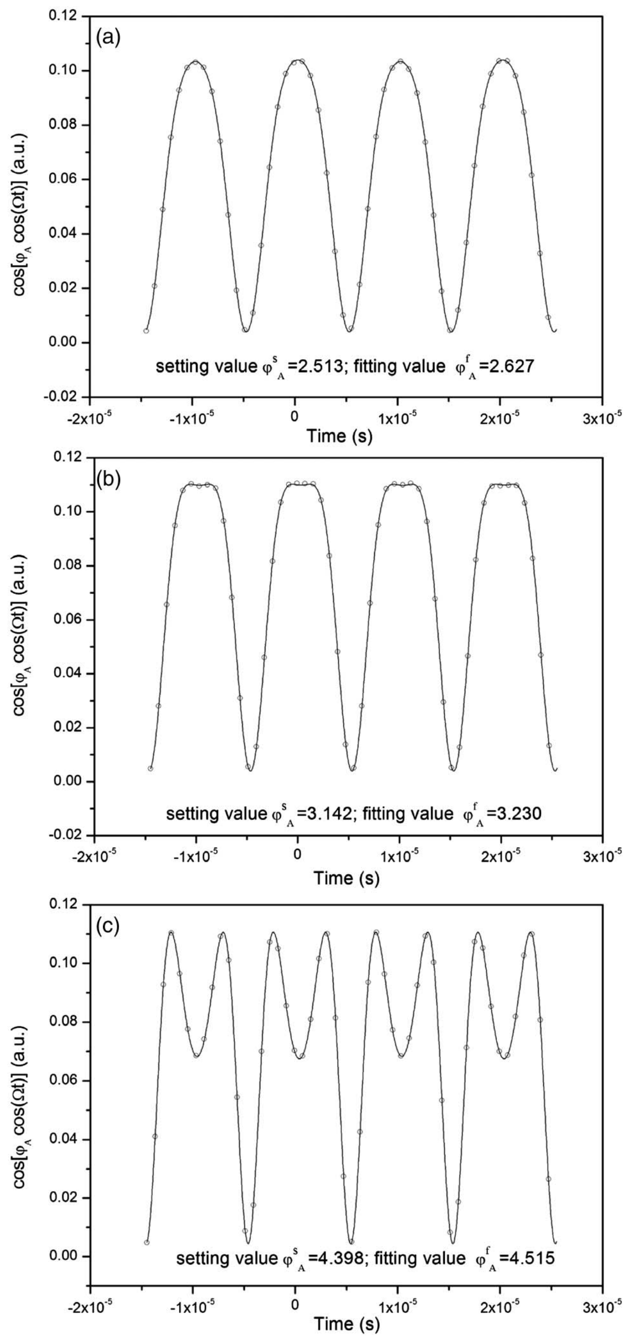

Fig. 3. Digitized oscilloscope waveforms (open circles) versus fitting waveforms (solid lines) with modulation amplitude setting values φ_A^s and fitting values φ_A^f being (a) $\varphi_A^s = 2.513$, $\varphi_A^f = 2.627$; (b) $\varphi_A^s = 3.142$, $\varphi_A^f = 3.230$; (c) $\varphi_A^s = 4.398$, $\varphi_A^f = 4.515$.

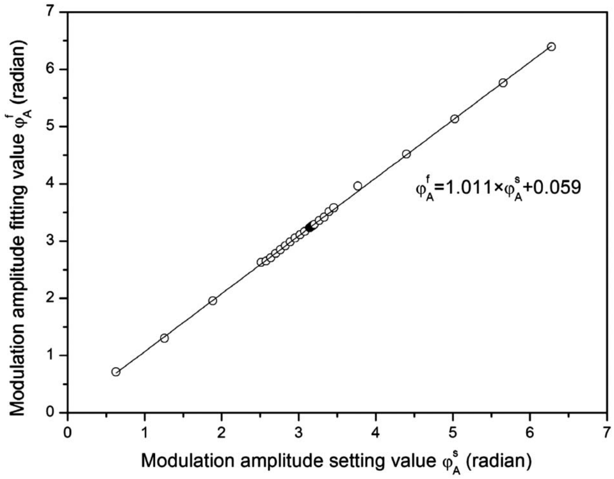

Fig. 4. Linear relationship between modulation amplitude setting values φ_A^s and fitting values φ_A^f.

relationship between φ_A^f and φ_A^s to be $\varphi_A^f = 1.011 \times \varphi_A^s + 0.059$, with φ_A^s increasing from zero to 2π.

We confirmed the accuracy of the curve-fitted φ_A values using a single-point calibration method and the fact that $J_2(\varphi_A)$ is zero when φ_A is equal to 5.136. We performed measurements with the same setup except that we replaced the oscilloscope with lock-in amplifiers. We set φ_A^s from 4.9 to 5.1 in increments of 0.01 and recorded the second harmonic $I_0\eta_2 J_2(\varphi_A)$ with the lock-in amplifier, which changed from positive to negative. By fitting the measured $I_0\eta_2 J_2(\varphi_A^s)$ as a linear function of φ_A^s, we found that $I_0\eta_2 J_2(\varphi_A^s) = -70.415 \times \varphi_A^s + 353.437$, as shown in Fig. 5. It vanishes when φ_A^s is 5.019. Based on the curve-fitting calibration method, this corresponds to an actual $\varphi_A^f = 5.133$, 0.003 or 0.06% from the value $\varphi_A = 5.136$ that makes $J_2(\varphi_A)$ vanish. This demonstrates the accuracy of the curve-fitting calibration method.

Equations (2) and (3) are derived assuming the phase retardation from the PEM has the form $\varphi = \varphi_A \cos \Omega t$. However, there exists a static birefringence in the PEM so that a static

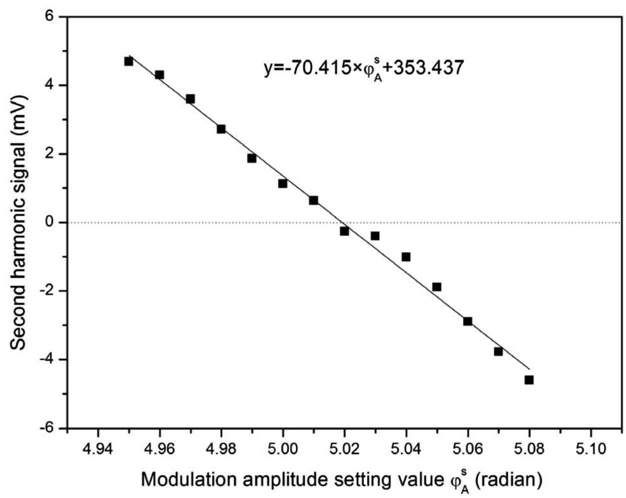

Fig. 5. Linear relationship between the second harmonic amplitude with modulation amplitude φ_A^s around zero values of $J_2(\varphi_A^s)$.

phase retardation φ_0 is present when the PEM is not resonantly driven by an alternating transducer [28–31]. Replacing $\varphi = \varphi_A \cos \Omega t$ with $\varphi = \varphi_0 + \varphi_A \cos \Omega t$ to take into account this static birefringence, the detected ellipsometry signal, Eq. (9), is now expressed as

$$I(t) = \frac{I_0}{2}[1 - \cos(\varphi_0 + \varphi_A \cos \Omega t)]$$
$$= \frac{I_0}{2}\left[\begin{array}{l} 1 - \cos \varphi_0 \eta_0 J_0(\varphi_A) + 2 \sin \varphi_0 \eta_1 J_1(\varphi_A) \cos \Omega t + \\ 2 \cos \varphi_0 \eta_2 J_2(\varphi_A) \cos 2\Omega t + \text{higher terms} \cdots \end{array}\right]. \quad \textbf{(10)}$$

For ideal modulators ($\varphi_0 = 0$), there is no first harmonic in the signal [Eq. (9)]; whereas for actual modulators ($\varphi_0 \neq 0$), $\sin \varphi_0$ is finite leading to a non-zero first harmonic in Eq. (10). φ_0 can be derived from the ratio of the first harmonic amplitude ($2 \sin \varphi_0 \eta_1 J_1(\varphi_A)$) to the second harmonic amplitude ($2 \cos \varphi_0 \eta_2 J_2(\varphi_A)$). To simplify the analysis, we set $\varphi_A^s = 2.544$ to have $\varphi_A^f = 2.631$ with which $J_1(\varphi_A^f) = J_2(\varphi_A^f)$. With $\eta_1/\eta_2 = 1.36$ (described in the following section), we find $\tan \varphi_0$ for our present PEM to be 0.011, which is consistent with previously reported findings [28,32].

The small static phase retardation φ_0 introduced by the PEM used does not affect the information on the molecular layer from OI-RD signals. In the presence of a non-zero static phase retardation φ_0, the first and the second harmonic of the OI-RD signal can be expressed as

$$I(\Omega) = -I_0 \eta_1 J_1(\varphi_A)|r_p||r_s| \sin(\delta - \Phi_{ps} - \Phi_{sys} - \varphi_0), \quad \textbf{(11)}$$

$$I(2\Omega) = I_0 \eta_2 J_2(\varphi_A)|r_p||r_s| \cos(\delta - \Phi_{ps} - \Phi_{sys} - \varphi_0). \quad \textbf{(12)}$$

During the nulling step, the first harmonic becomes zero on a bare substrate surface with $\Phi_{ps} = \delta_0 - \Phi_{sys} - \varphi_0$. Thus, the static phase retardation φ_0 only changes the phase difference Φ_{ps} of the phase shifter that is required to null the first harmonic signal from a bare substrate. The subsequent first harmonic is still proportional to $\sin(\delta - \delta_0)$, and the second harmonic amplitude of the molecular layer is proportional to $\cos(\delta - \delta_0)$, which are the same as the results when $\varphi_0 = 0$ in the PEM crystal.

It is easy to see that the above calibration methods for the modulation amplitude φ_A and the static phase retardation φ_0 are not affected by errors in azimuths of the polarizer and the analyzer shown in Fig. 2, while they are required to be at exactly $P = 45°$ and $A = 135°$ relative to the modulator axis in some calibration methods [23,33]. The light intensity reaching the detector in Fig. 2 is expressed as a function of azimuths P and A as

$$I(t) = I_0\left\{\cos^2(A-P) + \frac{\sin 2A \sin 2P}{2}[\cos(\varphi_0 + \varphi_A \cos \Omega t) - 1]\right\}$$
$$= I(dc) + I(\Omega)\cos \Omega t + I(2\Omega)\cos 2\Omega t + \text{higher term}, \quad \textbf{(13)}$$

$$I(dc) = \eta_0 I_0 \left\{\cos^2(A - P) + \frac{\sin 2A \sin 2P}{2}[\cos \varphi_0 J_0(\varphi_A) - 1]\right\}, \quad \textbf{(14)}$$

$$I(\Omega) = -\eta_1 I_0 \sin 2A \sin 2\mathrm{PJ}_1(\varphi_A) \sin \varphi_0, \quad (15)$$

$$I(2\Omega) = -\eta_2 I_0 \sin 2A \sin 2\mathrm{PJ}_2(\varphi_A) \cos \varphi_0. \quad (16)$$

Equations (13)–(16) show that the waveform of $\cos(\varphi_0+\varphi_A \cos \Omega t)$, the zero point of the second harmonic, and the ratio of the first harmonic to the second harmonic are all independent of azimuths P and A.

4. CALIBRATING AZIMUTHS OF POLARIZING OPTICS

Typically, setting azimuths of polarizing optics in ellipsometry is accomplished by finding nulls of suitable signals at special azimuth values [31,32,34–36]. Similarly here, without a phase shifter ($PS = 0°$, $\Phi_{ps} = 0°$), we can express the first and the second harmonic of an OI-RD signal as a function of the azimuths as follows from Eqs. (7) and (8):

$$I(\Omega) = -I_0\eta_1 J_1(\varphi_A) \sin 2(M - P) \sin 2A|r_p||r_s| \sin(\delta - \Phi_{sys}), \quad (17)$$

$$I(2\Omega) = -I_0\eta_2 J_2(\varphi_A) \sin 2(M - P) \begin{bmatrix} \sin 2M(|r_p|^2 \cos^2 A - |r_s|^2 \sin^2 A) \\ - \cos 2M|r_p||r_s| \sin 2A \cos(\delta - \Phi_{sys}) \end{bmatrix}. \quad (18)$$

P, M, and A are nominally set at 45°, 0°, and 135°, respectively, so that both the first harmonic and the second harmonic amplitude are non-zero. By adjusting A to null the first harmonic sets, $A = 0°$. With $A = 0°$, the second harmonic can be simplified as

$$I(2\Omega) = -I_0\eta_2 J_2(\varphi_A) \sin 2(M - P) \sin 2M|r_p|^2. \quad (19)$$

By nulling the second harmonic, we find the setting for $M = 0°$. Finally, keeping $M = 0°$, the analyzer A is rotated to 45° to make both the first and second harmonic finite. By rotating P to null both harmonics, we find the setting for $P = 0°$.

With $P = 45°$, $M = 0°$, and $A = 0°$, we inserted a phase shifter between the PEM and the sample. The first harmonic and the second harmonic in Eqs. (7) and (8) are now functions of the azimuth of the phase shifter PS and Φ_{ps};

$$I(\Omega) = I_0\eta_1 J_1(\varphi_A)|r_p|^2 \sin 2PS \sin \Phi_{ps}, \quad (20)$$

$$I(2\Omega) = \frac{1}{2} I_0\eta_2 J_2(\varphi_A)|r_p|^2 \sin 4PS(\cos \Phi_{ps} - 1). \quad (21)$$

By changing PS to null both harmonics, we find the setting for $PS = 0°$. With PS away from 0°, we find the setting for $\Phi_{ps} = 0°$.

After the calibration of the azimuths, one can then set $P = 45°$, $PS = 0°$, $M = 0°$, and $A = 135°$ and have the first harmonic proportional to $\sin(\delta - \delta_0)$ and the second harmonic proportional to $\cos(\delta - \delta_0)$. Deviations of PS and M from 0° introduce extra terms in both harmonics, making the absolute extraction of $\sin(\delta - \Phi_{ps} - \Phi_{sys})$ and $\cos(\delta - \Phi_{ps} - \Phi_{sys})$ from Eqs. (2) and (3) inaccurate. But if one only follows the changes in both harmonics as a result of surface processes, these extra terms do not have the effects if the deviations are small. We note that deviations of P and A from the specified values do not have such effects. The azimuths of $P = 45°$ and $A = 135°$ only maximize the overall signals.

5. MEASUREMENT OF THE AMPLICATION FACTOR RATIO η_1/η_2

In an OI-RD system, the first harmonic (e.g., 50 kHz) and the second harmonics (e.g., 100 kHz) are measured with an electronic transducer that converts the photocurrent signal from a photodetector to a voltage signal, filters out the dc component, and amplifies the ac components for subsequent phase-sensitive detection with lock-in amplifiers. As shown in Eqs. (2) and (3), the amplification factor that includes the transmission of the cable between the transducer and the lock-in amplifier is frequency dependent, η_1 for the first harmonic at 50 kHz and η_2 for the second harmonic at 100 kHz. As a result, η_1/η_2 needs to be measured for the accurate calculation of $\delta - \delta_0$. We measured η_1/η_2 from the ratio of the first harmonic maximum $(I_0\eta_1 J_1(\varphi_A)|r_p||r_s|)$ to the second harmonic maximum $(I_0\eta_2 J_2(\varphi_A)|r_p||r_s|)$ using a special value of modulation $\varphi_A^f = 2.631$ such that $J_1(2.631) = J_2(2.631)$. Then, we inserted a phase shifter (a Berek compensator, 5540, Newport, USA) between the PEM and the sample that adds an extra phase difference Φ_{ps}. As shown in Fig. 6, the first harmonic (filled triangles) and the second harmonic (empty circles) reach the maxima at respective Φ_{ps}. From these maxima, we find η_1/η_2 to be 1.36.

We define a total intensity maximum I_{max} as

$$I_{max} = \sqrt{[I(\Omega)]^2 + (\eta_1/\eta_2)^2[I(2\Omega)]^2} = I_0\eta_1 J_1(\varphi_A)|r_p||r_s|. \quad (22)$$

From Eq. (22), I_{max} should not be dependent on Φ_{ps}. To check the validity of this expected result, we calculated I_{max} from the measured $I(\Omega)$, $I(2\Omega)$, and η_1/η_2 (from the ratio of the maxima of both harmonics) and displayed the result in Fig. 6 (open triangles) as well. The calculated I_{max} is indeed constant of Φ_{ps} within 1%.

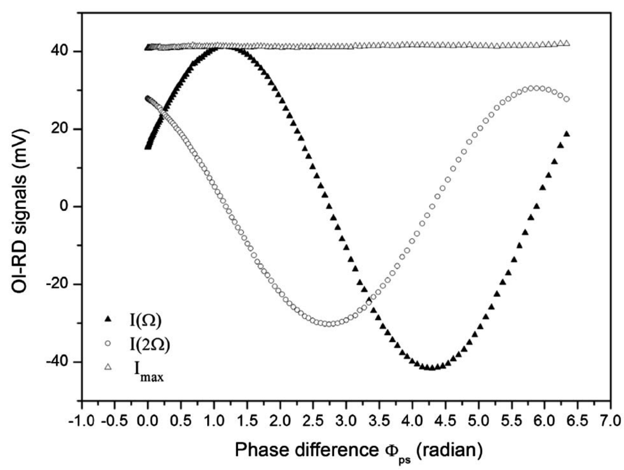

Fig. 6. Variation of the first harmonic amplitude $I(\Omega)$, second harmonic amplitude $I(2\Omega)$, and total intensity maximum I_{max} with phase difference Φ_{ps} of the phase shifter.

6. COMPARISONS OF FIRST HARMONIC NORMALIZATION METHODS

To deduce $\Delta\delta = \delta - \delta_0$ from an OI-RD ellipsometry measurement using Eq. (4), there are two methods to determine the pre-factor $I_0\eta_1 J_1(\varphi_A)$. The first method, as used by Zhu and coworkers so far, divides the first harmonic in Eq. (4) by the maximum of Eq. (2) $I_0\eta_1 J_1(\varphi_A)|r_{p0}||r_{s0}|$ on the bare substrate by adjusting the phase shifter Φ_{ps}. The normalized first harmonic is $|r_p||r_s|\sin(\delta - \delta_0)/(|r_{p0}||r_{s0}|)$. In the second method, as also used by Zhu and coworkers, the first harmonic in Eq. (4) is divided by the simultaneously measured second harmonic in Eq. (5) to yield $\tan(\delta - \delta_0)$. When the molecular layer thickness d is much less than wavelength λ, both methods give the same results, since $|r_p||r_s|$ is almost the same as $|r_{p0}||r_{s0}|$ from the bare substrate. When $|r_p||r_s|$ is not equal to $|r_{p0}||r_{s0}|$ anymore, the second method provides a more accurate measurement of $\Delta\delta = \delta - \delta_0$, as demonstrated in the next paragraphs.

To compare these two normalization methods experimentally, we fabricated a microarray of biotin-labeled bovine serum albumin (BBSA) printed on epoxy-functionalized glass slides. At printing concentrations of 0.94, 1.88, 3.75, 7.5, 15, and 30 μM, we printed four spots to form a row. The images of the microarray in the first harmonic and second harmonic of the OI-RD signal are shown in Fig. 7. For the second harmonic image, we see no noticeable features above the background when the printing concentration of the BBSA is equal to or less than 7.5 μM, indicating that $|r_p||r_s|$ from the BBSA-covered surface is almost identical to $|r_{p0}||r_{s0}|$ from the bare surface. For printing concentrations larger than 7.5 μM, we clearly see darker spots of printed BBSA, which indicates that $|r_p||r_s|$ from the BBSA-covered surface is less than $|r_{p0}||r_{s0}|$ from the bare surface.

The first harmonic normalized against the maximum from the bare surface, $|r_p||r_s|\sin(\delta - \delta_0)/(|r_{p0}||r_{s0}|)$, and the first harmonic normalized against the simultaneously measured second harmonic, $\tan(\delta - \delta_0)$, versus the BBSA printing concentration are plotted in Fig. 8. $|r_p||r_s|\sin(\delta - \delta_0)/(|r_{p0}||r_{s0}|)$ is almost identical to $\tan(\delta - \delta_0)$ when the printing concentration of BBSA is equal to or less than 7.5 μM. When the printing concentration further increases, $\tan(\delta - \delta_0)$ becomes larger than $|r_p||r_s|\sin(\delta - \delta_0)/(|r_{p0}||r_{s0}|)$. This is expected as $|r_p||r_s|$ is now smaller than $|r_{p0}||r_{s0}|$ and shows that the second normalization method, having the first harmonic signal normalized against the simultaneously measured second harmonic, provides a more accurate detection of $\tan(\delta - \delta_0)$.

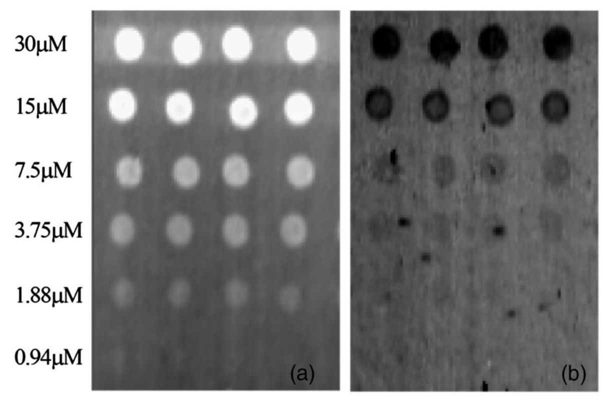

Fig. 7. Label-free OI-RD images of (a) the first harmonic amplitude and (b) the second harmonic amplitude for the BBSA microarray.

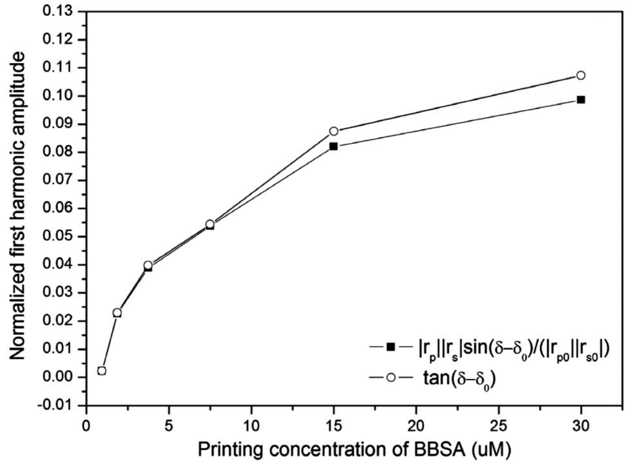

Fig. 8. Comparisons of the first harmonic amplitude normalized against the first harmonic maximum from a bare substrate $|r_p||r_s|\sin(\delta - \delta_0)/(|r_{p0}||r_{s0}|)$ with the first harmonic amplitude normalized against the simultaneously measured second harmonic amplitude $\tan(\delta - \delta_0)$.

7. DISCUSSION AND CONCLUSIONS

As a form of ellipsometry, the OI-RD technique characterizes properties of a biomolecular layer on a transparent solid substrate by measuring $\delta - \delta_0$, which is related to the biomolecular layer thickness d or its surface mass density through Eq. (6). Such an optical characterization does not require biomolecules to be labeled with tags of any kind. The OI-RD ellipsometry has been used to both qualitatively and quantitatively characterize ultrathin films of solid materials and biomolecular layers (e.g., small organic molecules, DNA fragments, proteins and protein fragments, viruses, and bacteria) on solid surfaces with remarkable versatility and accuracy [13–20]. With polarizer azimuth P at 45°, PEM azimuth M at 0°, phase shifter azimuth PS at 0°, analyzer azimuth A at 135°, the OI-RD signals are related to $\delta - \delta_0$ through Eqs. (3) and (4). To precisely determine $\delta - \delta_0$, the parameters of the polarizing optics need to be calibrated and set accurately.

The modulation amplitude φ_A of the PEM affects the amplitude of the first and the second harmonic signals, and in turn affects the accuracy of $\delta - \delta_0$. Currently, single-point calibration methods are widely used to calibrate the modulation amplitude φ_A. Some single-point methods are based on the observation of distinctive waveforms on the oscilloscope, some methods are based on finding set points where the Bessel functions produced by the harmonic signals are equal to zero. One limitation of the single-point methods is that only one calibration point may be obtained when distinctive waveforms appear or the Bessel functions cross zero. Therefore, a more encompassing calibration must be used to combine several single-point calibration methods together, where different measurement setups are usually involved. In this manuscript, we described a curve-fitting procedure to determine the modulation amplitude φ_A of a PEM in an OI-RD system, which could produce calibration curves over the entire usable range of the modulator. Compared to the single-point calibration method, the curve-fitting method is able to determine φ_A with an accuracy of 0.003 radians. We also showed that the static phase retardation φ_0 can be determined by the ratio of a suitable first harmonic to the corresponding second harmonic of the OI-RD signal, and more importantly φ_0 has no effect on the extraction of $\delta - \delta_0$.

The azimuths of polarization optics can cause significant deviation of OI-RD signals from $\delta - \delta_0$. With arbitrary azimuths for polarization optics, OI-RD signals are expressed as Eqs. (7) and (8), instead of Eqs. (3) and (4). We described a set of sequential procedures to precisely set azimuths of polarizer P, analyzer A, PEM M, and phase shifter PS. Deviations of PS and M away from ideally set values would add extra terms, making the absolute extraction of $\delta - \Phi_{ps} - \Phi_{sys}$ inaccurate. However, if one only follows the change in the OI-RD signal after nulling, these extra terms do not affect the extraction of $\delta - \delta_0$ when the deviations are small. The errors in the azimuths of P and A only affect the absolute amplitudes of the first and second harmonic signals so that the calculation of $\delta - \delta_0$ is accurate after normalization. We explicitly show that by normalizing the first harmonic by the simultaneously acquired second harmonic gives a more accurate measurement of $\delta - \delta_0$ than the method of normalizing the first harmonic signal by the maximum of first harmonic signal from the bare surface obtained by adjusting the phase shifter.

Funding. National Natural Science Foundation of China (NSFC) (61505032, 11574056); Ministry of Education of the People's Republic of China (MOE); Shanghai Pujiang Program (13PJ1400300); Natural Science Foundation of Jiangsu Higher Education Institutions of China (BK20130116).

REFERENCES

1. D. L. Confer, R. M. A. Azzam, and N. M. Bashara, "Ellipsometer nulling: convergence and speed," Appl. Opt. **15**, 2568–2575 (1976).
2. S. Jasperson, D. K. Burge, and R. C. Ohandley, "A modulated ellipsometer for studying thin film optical properties and surface dynamics," Surf. Sci. **37**, 548–558 (1973).
3. A. Wong and X. D. Zhu, "An optical differential reflectance study of adsorption and desorption of xenon and deuterium on Ni(111)," Appl. Phys. A **63**, 1–8 (1996).
4. X. F. Jin, M. Y. Mao, S. Ko, and Y. R. Shen, "Adsorption and desorption kinetics of CO on Cu(110) studied by optical differential reflectance," Phys. Rev. B **54**, 7701–7704 (1996).
5. X. D. Zhu and E. Nabighian, "*In situ* monitoring of ion sputtering and thermal annealing of crystalline surfaces using an oblique-incidence optical reflectance difference method," Appl. Phys. Lett. **73**, 2736–2738 (1998).
6. E. Nabighian, M. C. Bartelt, and X. D. Zhu, "Kinetic roughening during rare-gas homoepitaxy," Phys. Rev. B **62**, 1619–1622 (2000).
7. P. Thomas, E. Nabighian, M. C. Bartelt, C. Y. Fong, and X. D. Zhu, "An oblique-incidence optical reflectivity difference and LEED study of rare-gas growth on a lattice-mismatched metal substrate," Appl. Phys. A **79**, 131–137 (2004).
8. X. D. Zhu, Y. Y. Fei, X. Wang, H. B. Lu, and G. Z. Yang, "General theory of optical reflection from a thin film on a solid and its application to heteroepitaxy," Phys. Rev. B **75**, 245434 (2007).
9. X. D. Zhu, S. Wicklein, F. Gunkel, R. Xiao, and R. Dittmann, "*In situ* optical characterization of $LaAlO_3$ epitaxy on $SrTiO_3$(001)," Europhys. Lett. **109**, 37006 (2015).
10. W. Schwarzacher, J. W. Gray, and X. D. Zhu, "Oblique incidence reflectivity difference as an *in situ* probe of Co electrodeposition on polycrystalline Au," Electrochem. Solid-State Lett. **6**, C73–C76 (2003).
11. G. Y. Wu, S. E. Bae, A. A. Gewirth, J. A. Gray, X. D. Zhu, T. P. Moffat, and W. Schwarzacher, "Pb electrodeposition on polycrystalline Cu in the presence and absence of Cl–: a combined oblique incidence reflectivity difference and *in situ* AFM study," Surf. Sci. **601**, 1886–1891 (2007).
12. Y. Y. Fei, Y. S. Sun, Y. H. Li, H. Yu, K. Lau, J. Landry, Z. Luo, N. Baumgarth, X. Chen, and X. D. Zhu, "Characterization of receptor binding profiles of influenza A viruses using an ellipsometry-based label-free glycan microarray assay platform," Biomolecules **5**, 1480–1498 (2015).
13. Y. Y. Fei, A. Schmidt, G. Bylund, D. X. Johansson, S. Henriksson, C. Lebrilla, J. V. Solnick, T. Boren, and X. D. Zhu, "Use of real-time, label-free analysis in revealing low-affinity binding to blood group antigens by helicobacter pylori," Anal. Chem. **83**, 6336–6341 (2011).
14. J. P. Landry, Y. Y. Fei, X. D. Zhu, Y. H. Ke, G. L. Yu, and P. Lee, "Discovering small molecule ligands of vascular endothelial growth factor that block VEGF-KDR binding using label-free microarray-based assays," Assay Drug Dev Technol. **11**, 326–332 (2013).
15. C. G. Zhu, X. D. Zhu, J. P. Landry, Z. M. Cui, Q. F. Li, Y. J. Dang, M. Lan, F. Y. Zheng, and Y. Y. Fei, "Developing an efficient and general strategy for immobilization of small molecules onto microarrays using isocyanate chemistry," Sensors **16**, 378 (2016).
16. Y. Y. Fei, J. P. Landry, Y. S. Sun, X. D. Zhu, J. T. Luo, X. B. Wang, and K. S. Lam, "A novel high-throughput scanning microscope for label-free detection of protein and small-molecule chemical microarrays," Rev. Sci. Instrum. **79**, 013708 (2008).
17. X. X. Guo, Y. H. Deng, C. G. Zhu, J. L. Cai, X. D. Zhu, J. P. Landry, F. Y. Zheng, X. J. Cheng, and Y. Y. Fei, "Characterization of protein expression levels with label-free detected reverse phase protein arrays," Anal. Biochem. **509**, 67–72 (2016).
18. X. D. Zhu, J. P. Landry, Y. S. Sun, J. P. Gregg, K. S. Lam, and X. W. Guo, "Oblique-incidence reflectivity difference microscope for label-free high-throughput detection of biochemical reactions in a microarray format," Appl. Opt. **46**, 1890–1895 (2007).
19. X. D. Zhu, "Comparison of two optical techniques for label-free detection of biomolecular microarrays on solids," Opt. Commun. **259**, 751–753 (2006).
20. J. P. Landry, X. D. Zhu, and J. P. Gregg, "Label-free detection of microarrays of biomolecules by oblique-incidence reflectivity difference microscopy," Opt. Lett. **29**, 581–583 (2004).
21. M. W. Wang, Y. F. Chao, K. C. Leou, F. H. Tsai, T. L. Lin, S. S. Chen, and Y. W. Liu, "Calibrations of phase modulation amplitude of photoelastic modulator," Jpn. J. Appl. Phys. **43**, 827–832 (2004).
22. T. C. Oakberg, J. Trunk, and J. C. Sutherland, "Calibration of photoelastic modulators in the vacuum UV," Proc. SPIE **4133**, 101–111 (2000).
23. M. W. Wang, F. H. Tsai, and Y. F. Chao, "*In situ* calibration technique for photoelastic modulator in ellipsometry," Thin Solid Films **455**, 78–83 (2004).
24. "PEM-100 photoelastic modulator user manual," P/N: 010-0000-021 UM Rev H (Hinds Instruments, 2013).
25. J. C. Cheng, L. A. Nafie, S. D. Allen, and A. I. Braunstein, "Photoelastic modulator for 0.55-13-μm range," Appl. Opt. **15**, 1960–1965 (1976).
26. K. J. Braun, C. R. Lytle, J. A. Kavanaugh, J. A. Thielen, and A. S. Green, "A simple, inexpensive photoelastic modulator," Am. J. Phys. **77**, 13–19 (2009).
27. G. E. Jellison, F. A. Modine, and C. Chen, "Calibration procedures for a two-modulator generalized ellipsometer," Proc. SPIE **3754**, 150–160 (1999).

28. J. M. DiNitto and J. M. Kenney, “Novel technique for improvement in calibration of the photoelastic modulator in circular and linear dichroism spectroscopy,” Appl. Spectrosc. **67**, 40–48 (2013).
29. O. Acher, E. Bigan, and B. Drevillon, “Improvement of phase-modulated ellipsometry,” Rev. Sci. Instrum. **60**, 65–77 (1989).
30. Y. F. Chao and P. L. Lin, “Artifactual circular dichroism effect in a photoelastic modulator,” Opt. Commun. **283**, 4582–4585 (2010).
31. K. Postava, A. Maziewski, T. Yamaguchi, R. Ossikovski, S. Visnovsky, and J. Pistora, “Null ellipsometer with phase modulation,” Opt. Express **12**, 6040–6045 (2004).
32. J. G. E. Jellison and F. A. Modine, “Accurate calibration of a photoelastic modulator in polarization modulation ellipsometry,” Proc. SPIE **1166**, 231–241 (1990).
33. A. J. Zeng, L. H. Huang, Z. R. Dong, J. M. Hu, H. J. Huang, and X. Z. Wang, “Calibration method for a photoelastic modulator with a peak retardation of less than a half-wavelength,” Appl. Opt. **46**, 699–703 (2007).
34. J. R. Adams and N. M. Bashara, “In process ellipsometer azimuth angle calibration,” Appl. Opt. **15**, 3179–3184 (1976).
35. J. M. M. de Nijs, A. H. M. Holtslag, A. Hoeksta, and A. van Silfhout, “Calibration method for rotating-analyzer ellipsometers,” J. Opt. Soc. Am. A **5**, 1466–1471 (1988).
36. B. Drevillon, J. Perrin, R. Marbot, A. Violet, and J. L. Dalby, “Fast polarization modulated ellipsometer using a microprocessor system for digital Fourier analysis,” Rev. Sci. Instrum. **53**, 969–977 (1982).